Density Functional Study on the Geometric Features and Growing Pattern of B_nP_m Clusters with $n = 1–4$, $m = 1–4$, $n + m \leq 5$

Verónica Ferraresi Curotto*[a] and Reinaldo Pis Diez*[b]

The bonding features of B_nP_m clusters ($n = 1–4$, $m = 1–4$, $n + m \leq 5$) are studied within the framework of the density functional theory following a systematic growing mechanism. Some stable geometries are found to agree well with results reported previously in the literature. Other geometries are found to be more stable than structures reported elsewhere for small B/P aggregates. To the best of our knowledge, stable geometries for BP_4 are reported for the first time. It is found that small B/P clusters with up to five atoms tend to grow mainly toward nonlinear bidimensional structures. The existence of B—B and B—P bonds seems to be of importance for the relative stability of clusters as they grow. The growing patterns could be explained mainly in terms of electrophilic attacks of B atoms to B—B and B—P bonds. It is found that the growing is in general accompanied by geometry reorganization and atomic charge rearrangements. Electrophilic attacks of P atoms to B—B bonds seems to be a good alternative to grow for aggregates with many B atoms. Atomic charges derived from molecular electrostatic potentials are useful to understand the growing paths followed in terms of electrophilic or nucleophilic attacks. © 2012 Wiley Periodicals, Inc.

DOI: 10.1002/qua.24194

Introduction

Boron and phosphorus compounds are considered systems of interest in solid-state physics and chemistry because of their potential use as refractory materials. The few experimental studies found so far are focused in obtaining stable structures by means of vapor deposition and in characterizing them by spectroscopic techniques.[1,2]

Theoretical studies, conversely, are focused in studying stabilities, equilibrium structures, and vibrational modes of small binary clusters. Linguerri and coworkers[3] studied different electronic states of BP, BP^+, BP^-, B_2P_2, $(B_2P_2)^+$, and $(B_2P_2)^-$ using the CCSD method and a cc-pVQZ basis set. Qu and coworkers[4] investigated the electronic structures and stabilities of $(BP)_n$ aggregates, where $n = 2–4$, using the hybrid exchange-correlation B3LYP functional and 6-31G(d) and 6-311++G(2d) basis sets. Shi et al.[5] used the CCSD(T)/6-311+G(d)//B3LYP/6-311+G(d) level of theory to study structures, potential energy surfaces, growth patterns, and stabilities of planar B_nP clusters, with $n = 1–7$. Burrill and Grein[6] studied structural properties of X_2Y_2 (X = B, Al, Ga; Y = N, P, As) aggregates using both the B3LYP and MP2 methods with a 6-311+G(3df) basis set. Gan et al.[7] used the full (CI) and CCSD(T) methodologies with cc-pVTZ correlation consistent basis sets to investigate the properties of groups III/V diatomic molecules BN, BP, AlN, and AlP.

Clusters of B_nP_m stoichiometry ($n = 1–4$, $m = 1–4$, $n + m \leq 5$) are studied in this work within the framework of the density functional theory, paying special attention to the form in which clusters grow when new atoms are added up. To the best of our knowledge, this is the first work in which a systematic investigation of the growing features of both two-dimensional (2D) and 3D B/P clusters is carried out. Moreover, geometric parameters, atomization energies, and electron spin multiplicities are also reported for the more stable clusters of each size.

Computational Methods

B_nP_m clusters ($n = 1–4$, $m = 1–4$, $n + m \leq 5$) are studied in this work using tools from the density functional theory.[8–10] The three-parameter hybrid exchange-correlation B3LYP functional is used.[10–12] Correlation-consistent basis sets of triple-ζ quality, augmented with polarization functions are used for both B and P.[13,14]

Geometry optimizations are performed using the heteronuclear diatomic aggregate, BP, as a starting point. Then, both B and P atoms are added up one at a time to form larger clusters with a maximum of five atoms. As every new atom could enter on-top, bridge or hollow sites, various starting geometries are considered for optimization of every new cluster size. The growing pattern is constructed according to the increase

[a] V. F. Curotto
Departamento de Química, Facultad de Ciencias Exactas y Naturales, Universidad Nacional de Catamarca, Av. Belgrano 300, K4700AAP Catamarca, Argentina
E-mail: vferraresi@conicet.gov.ar

[b] R. P. Diez
CEQUINOR, Centro de Química Inorgánica (CONICET, UNLP), Departamento de Química, Facultad de Ciencias Exactas, Universidad Nacional de La Plata CC 962, B1900AVV La Plata, Argentina
E-mail: pis_diez@quimica.unlp.edu.ar

Contract grant sponsors: CONICET, UNLP.

observed for the atomization energy per atom, which is defined as

$$E_{\text{atom}} = \frac{nE_{\text{B}} + mE_{\text{P}} - E_{\text{B}_n\text{P}_m}}{n+m}$$

where $E_{\text{B}_n\text{P}_m}$ is the total electronic energy of the corresponding conformer and E_{B} and E_{P} are the electronic energy of the atoms in their ground state. In this way, every cluster formed by N atoms is a candidate to grow only if its atomization energy per atom is greater than that of the aggregate formed by $N-1$ atoms from which it originates.

Geometry optimizations are performed without symmetry constraints. As the electron spin multiplicity remains fixed during the calculations, a series of geometry optimizations with varying multiplicities is performed for every cluster until the atomization energy per atom reaches its maximum value. The Hessian matrix of the total electronic energy with respect to nuclear coordinates is calculated and diagonalized to verify whether the optimized geometries are true minima or saddle points on the potential energy surface of the clusters.

To rationalize the growing pattern of B_nP_m clusters, both atomic charges derived from molecular electrostatic potentials (MEP-derived atomic charges) and spin densities (SD) per atom are calculated for every conformer. It was recently demonstrated that MEP-derived atomic charges reproduce very well the sites susceptible both to electrophilic and nucleophilic attacks that can be observed in MEP surfaces.[15] Moreover, MEP-derived atomic charges allow a quantitative ordering of those sites. SD surfaces are also very well described by the SD per atom.[15] These facts indicate that both MEP-derived atomic charges and SD per atom could be used instead of the corresponding molecular surfaces, retaining all their quantitative features at the same time. MEP-derived atomic charges are obtained according to the scheme proposed by Singh and Kollman and Merz[16,17] and SD are generated through an NBO analysis[18] performed on open-shell systems.

All calculations in this work are performed with the Gaussian 03 package,[19] whereas all figures are produced with the aid of the gOpenMol program.[20,21]

Results and Discussion

Geometries and atomization energies

Table 1 shows the results for BP and the BP_2 and B_2P triatomic clusters and Figure 1 shows their equilibrium geometries. As can be seen from the table, BP is characterized by a triplet ground state, in good agreement with results obtained by other authors.[3–5,7] The most stable BP_2 cluster is characterized by a doublet electronic state, whereas the B_2P ground state, conformer **4**, presents a triangular geometry, in agreement with results reported in Ref. [5]. A close examination to the topological features of the triatomic clusters suggests that their relative stability in energy could be associated to the formation of B—P and B—B bonds. In line with that suggestion, the P—P bond could be the responsible of the low atomization energy in conformer **3**.

Table 1. Atomization energies, E_{at} in eV/at, spin multiplicities, M_S, and symmetry for the stable B/P diatomic and triatomics found in this work.

Conformer		E_{at}	M_S	Symmetry
BP	**1**	1.75	3	$C_{\infty v}$
		−[3, 7]	3	
		− [4, 5]	3	$C_{\infty v}$
BP_2	**2**	2.58	2	$D_{\infty h}$
	3	2.00	2	C_s
B_2P	**4**	2.81	2	C_s
		− [5]	2	C_s
	5	2.64	2	$C_{\infty v}$

Comparison with results by other authors is made when available. A label is also shown in the second column, see text and Figure 1.

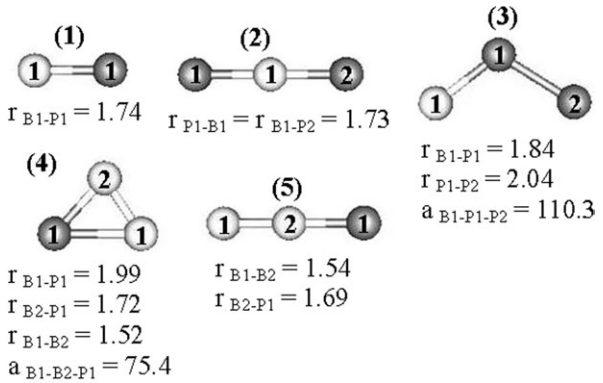

Figure 1. Equilibrium geometries of the stable diatomic and triatomics found for B/P aggregates. White and gray circles are boron and phosphorus atoms, respectively. Numbers in parenthesis are the cluster labels, see text and Table 1. Equilibrium bond distances are indicated in Å.

In the case of the tetratomic clusters, two stable conformers are obtained for BP_3 and B_3P, whereas six stable conformers are found for B_2P_2, see Table 2 and Figure 2. Two aggregates that show rhombus-like geometries, **6** and **14**, are BP_3 and B_3P ground states, respectively. Less stable tetratomic species, **7** and **15**, are found at about 0.35 eV/at lower in energy than the corresponding ground states. Interestingly, conformers **6**

Table 2. Atomization energies, E_{at} in eV/at, spin multiplicities, M_S, and symmetry for the stable B/P tetratomics found in this work.

Conformer		E_{at}	M_S	Symmetry
BP_3	**6**	3.05	1	C_1
	7	2.69	1	C_1
B_2P_2	**8**	3.11	3	$D_{\infty h}$
	9	3.03	3	C_1
	10	2.90	3	C_1
	11	2.87	3	C_1
		− [3, 4, 6]	3	D_{2h}
	12	2.62	3	C_1
	13	2.48	3	C_1
B_3P	**14**	3.24	3	C_1
		− [5]	1	C_{2v}
	15	2.89	3	$C_{\infty v}$

Comparison with results by other authors is made when available. A label is also shown in the second column, see text and Figure 2.

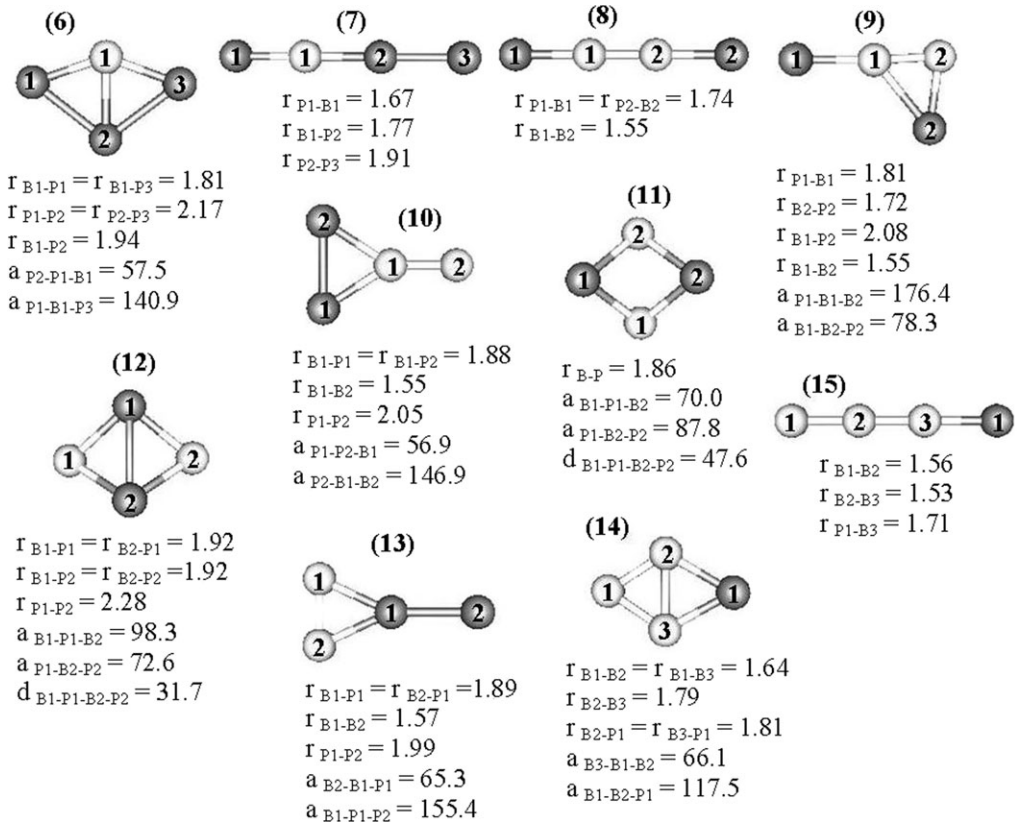

Figure 2. Equilibrium geometries of the stable tetratomics found for B/P aggregates. White and gray circles are boron and phosphorus atoms, respectively. Numbers in parenthesis are the cluster labels, see text and Table 2. Equilibrium bond distances, *r*, are indicated in Å and bond angles, *a*, and torsion angles, *d*, are shown in degrees, respectively. Bond angles not shown are equal to 180○. Torsion angles are not provided in the case of planar aggregates.

and **7** are characterized by a singlet electronic state, whereas conformers **14** and **15** exhibit a triplet electronic state. This fact is in disagreement with results reported in Ref. [5], in which a singlet electronic state is predicted to be the ground state of B_3P. The six stable species of B_2P_2 are characterized by a triplet electronic state. A linear aggregate, conformer **8**, is found to be the ground state of B_2P_2. It is worth mentioning that a rhombus-like structure, similar to that of conformer **11**, is reported as the more stable isomer in Refs. [3, 4, 6]. Conformer **11** is 0.24 eV/at lower in energy than conformer **8** in this work. A close examination of the topological features of the tetratomic clusters suggests that their relative stability depends on the number of B—P and B—B bonds, see conformers **8**, **9**, and **14**. Interestingly, conformer **6** is one of the more stable tetratomic clusters and presents two P—P bonds, see Figure 2. However, a detailed inspection to the geometric features of that conformer shows that the P—P bonds are considerably longer than P—P bonds in other tetratomic aggregates like **7**, **10**, or **13**, in which the P—P distance range from 1.91 to 2.05 Å. Incidentally, atomization energies of these three conformers are much lower than the atomization energy of the most stable tetratomic aggregates. These findings seem to suggest that P—P bond distances shorter than 2.05 Å contribute to decrease the relative stability of small B/P aggregates.

Table 3 lists the stable conformations found for the different pentatomic clusters studied in this work. Figures 3–5 show their corresponding equilibrium geometries. Eight stable conformers are found for B_2P_3, nine and five stable species are obtained for B_3P_2 and for B_4P, respectively, and four stable structures are achieved for BP_4. The ground state of B_2P_3, conformer **16**, is characterized by a doublet electronic state and a 3D structure with a slightly distorted trapezoidal geometry, see Figure 3. Interestingly, all stable B_2P_3 conformers present nonlinear equilibrium structures and only conformers **17** and **23** show 2D geometries. The ground state of B_3P_2, conformer **24**, is found to be a doublet electronic state and its equilibrium geometry is characterized by a slightly distorted 2D trapezoid, see Figure 4. Conformer **27** is the only linear B_3P_2 conformer, whereas conformers **28**, **31**, and **32** are the only 3D structures. Despite the similar equilibrium geometries of conformers **31** and **32**, it is worth noting that they originate from different starting structures. All stable B_4P clusters adopt 2D structures, see Figure 5. Conformer **33** becomes the B_4P ground state, being characterized by a doublet electronic state, in agreement with Ref. [5]. Finally, conformer **38** is found to be the ground state of BP_4. It is characterized by a doublet electronic state and a 3D equilibrium geometry. Conformer **39** also presents a 3D equilibrium geometry, whereas conformers **40** and **41** are characterized by planar structures. The four stable BP_4 conformers exhibit very low atomization energies. It is worth emphasizing that to the best of our knowledge this is the first report of stable BP_4 pentatomic aggregates. It is interesting to mention that conformers **33** and **24**, the pentatomic species with the higher atomization energies, are dominated

Table 3. Atomization energies, E_{at} in eV/at, spin multiplicities, M_S, and symmetry for the stable B/P pentatomics found in this work.

Conformer		E_{at}	M_S	Symmetry
B_2P_3	**16**	3.35	2	C_1
	17	3.32	2	C_1
	18	3.26	2	C_1
	19	3.01	2	C_1
	20	3.00	4	C_1
	21	2.96	4	C_1
	22	2.92	4	C_1
	23	2.55	2	C_1
B_3P_2	**24**	3.70	2	C_1
	25	3.45	2	C_1
	26	3.37	2	C_1
	27	3.35	2	C_1
	28	3.32	2	C_1
	29	3.31	2	C_1
	30	3.17	4	C_1
	31	2.98	2	C_1
	32	2.96	2	C_1
B_4P	**33**	3.73	2	C_1
		−[5]	2	C_s
	34	3.50	4	C_1
	35	3.40	4	C_1
	36	3.25	4	C_1
	37	3.25	4	C_1
BP_4	**38**	2.97	2	C_1
	39	2.79	4	C_1
	40	2.67	2	C_1
	41	2.67	4	C_1

Comparison with results by other authors is made when available. A label is also shown in the second column, see text and Figures 3–5.

by B—B and B—P bonds. A second set of pentatomic clusters, with atomization energies ranging from 3.50 to 3.25 eV/at, consists of conformers **16**–**18**, **25**–**29**, and **34**–**37**. These species are mainly dominated by B—P bonds, with a minor contribution from B—B bonds. In the few cases in which P—P bonds are also present, the bond distances are larger than 2.05 Å, thus reinforcing the proposed argument that short P—P bonds could be responsible for the lower relative stability of B/P aggregates.

The growing patterns of B—P clusters

Growing patterns are studied taking the BP diatomic cluster as starting point. Seeking for simplicity, only those aggregates lying up to 0.15 eV below the ground state of every cluster size are considered as potential candidates to grow. According to the Maxwell–Boltzmann distribution, such a difference is equivalent to a contribution of the given conformer of about 5% to every cluster property measured at a temperature of 600 K.

It can be seen from Table 4 that conformer **2**, the most stable BP_2 species, originates as a consequence of a nucleophilic attack to the B atom in the diatomic cluster. Conversely, the most stable B_2P aggregate, conformer **4**, is formed after an electrophilic attack to the B—P bond in the diatomic cluster. The other conformers, **3** and **5**, lie above the threshold of 0.05 eV/at (0.15 eV/3 atoms) and are not considered as candidates to grow. It is interesting to note that a considerable electronic charge rearrangement takes place when conformer **2** is formed. The two P atoms become sites susceptible of nucleophilic attacks, whereas the central B atom becomes a site susceptible of electrophilic attacks. When conformer **4** is formed, an appreciable charge transfer occurs from the P atom in the diatomic species to the incoming B atom. As a consequence of that, the P atom becomes a site susceptible of nucleophilic attacks, whereas the B atoms become sites susceptible both of electrophilic and nucleophilic attacks. Interestingly, all triatomic aggregates exhibit a decrease in the electron spin multiplicity with respect to the diatomic aggregate, indicating that electrons tend to pair each other during the growing. This finding is consistent with the decrease in the SD per atom observed in **2** and **4**.

It can be seen from Table 2 that the ground states of BP_3, B_2P_2, and B_3P, conformers **6**, **8**, and **14**, respectively, are separated by low-lying excited states by more than 0.04 eV/at, the threshold arbitrarily imposed before. Thus, only those three tetratomic clusters are considered as candidates for growing from the most stable triatomic aggregates. The comparison of equilibrium geometries of conformers **2** and **6**, see Figures 1 and 2 and Table 5, suggests that the growing occurs through an electrophilic attack of the incoming P atom to the B atom in **2**. However, the final MEP-derived atomic charges on conformer **6** would indicate whether a quite different growing mechanism or an important charge rearrangement during growing. Conformer **8** is able to grow both from **2** and **4**. The criterion of an increase in the atomization energy seems to favor the **2** → **8** route. Moreover, a close inspection to the three structures involved on the growing suggests that **8** grows from conformer **2** as a consequence of an electrophilic attack of a B atom to a B—P bond, which becomes completely broken in the final conformer giving place to a new B—P bond and to a brand new B—B bond. Conversely, it is argued that a B—P bond in **4** is broken due to an electrophilic attack by a P atom and an important geometry rearrangement leads to a new B—P bond. Thus, both arguments seem to favor the **2** → **8** growing path, mainly due to the formation of a B—B bond. Conformer **14** grows from **4** as a consequence of an electrophilic attack of a B atom to a B—B bond. MEP-derived atomic charges confirm the mechanism above. SD per atom values show that unpaired electrons tend to remain localized into P atoms in conformer **8** and into B atoms in **14**. Conformer **6** exhibits a closed-shell electronic configuration.

Only pentatomic clusters **16**, **17**, **24**, and **33** are candidates to grow according to their atomization energies. Low-lying excited states lie above the 0.03 eV/at threshold arbitrarily imposed in this work. Conformers **38**–**41** are excluded from this study on growing patterns due to their low atomization energies. It is worth noting that **17** is the only excited state within the 0.03 eV/at threshold from the B_2P_3 ground state, conformer **16**. Conformer **16** could grow whether from conformer **6** or from conformer **8**. A close examination to the equilibrium structures and MEP derived atomic charges, Figures 2 and 3 and Table 6, indicates that the **6** → 16 route involves an electrophilic attack of a B atom to a P—P bond followed by an important atom reorganization and atomic charge rearrangement, which leads to an increase in the number of B—P bonds, the formation of an additional B—B bond

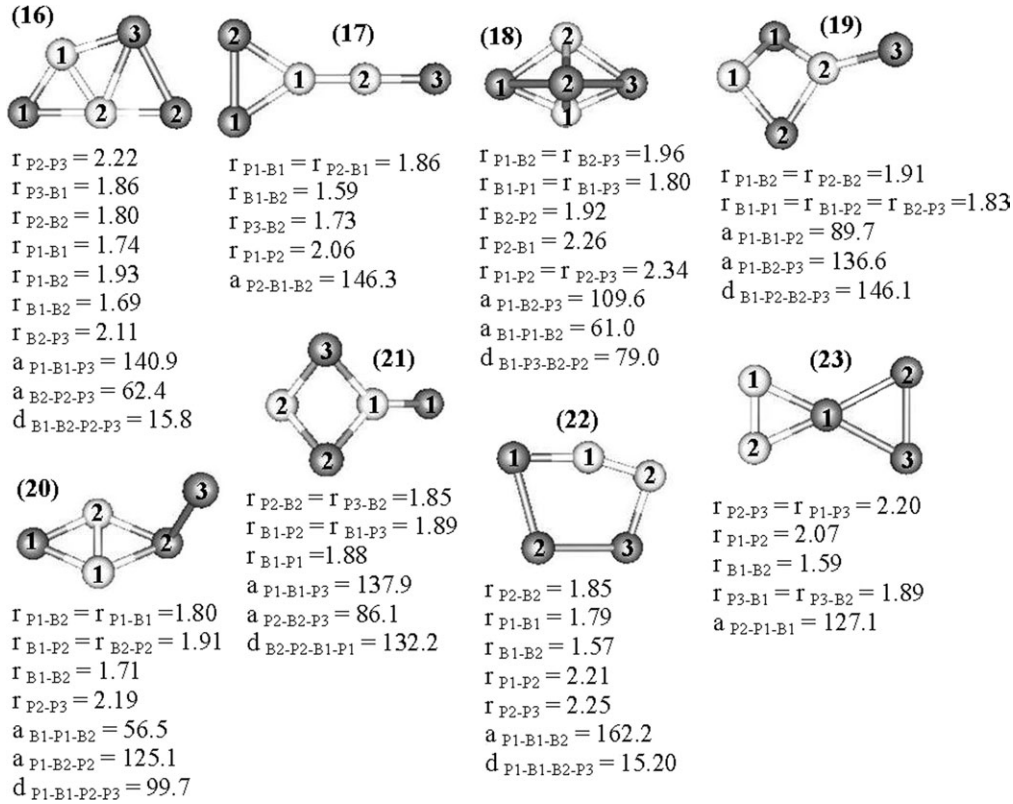

Figure 3. Equilibrium geometries of the stable B_2P_3 pentatomic aggregates. White and gray circles are boron and phosphorus atoms, respectively. Numbers in parenthesis are the cluster labels, see text and Table 3. Equilibrium bond distances, *r*, are indicated in Å and bond angles, *a*, and torsion angles, *d*, are shown in degrees, respectively. Bond angles not shown are equal to 180○. Torsion angles are not provided in the case of planar aggregates.

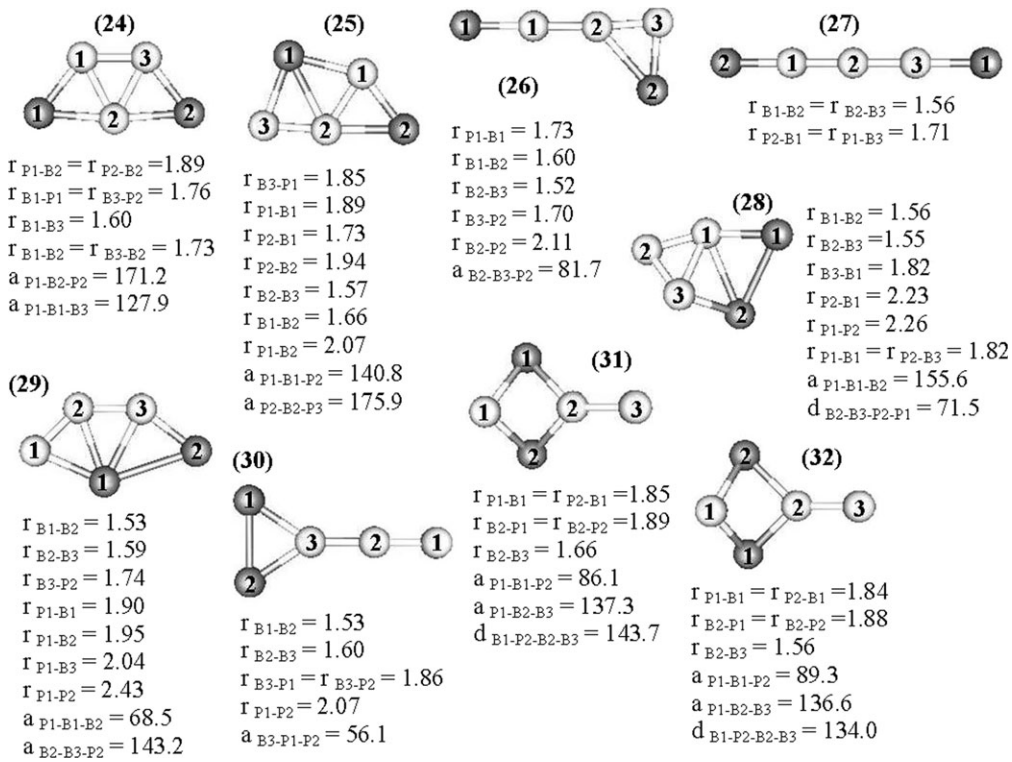

Figure 4. Equilibrium geometries of the stable B_3P_2 pentatomic aggregates. White and gray circles are boron and phosphorus atoms, respectively. Numbers in parenthesis are the cluster labels, see text and Table 3. Equilibrium bond distances, *r*, are indicated in Å and bond angles, *a*, and torsion angles, *d*, are shown in degrees, respectively. Bond angles not shown are equal to 180°. Torsion angles are not provided in the case of planar aggregates.

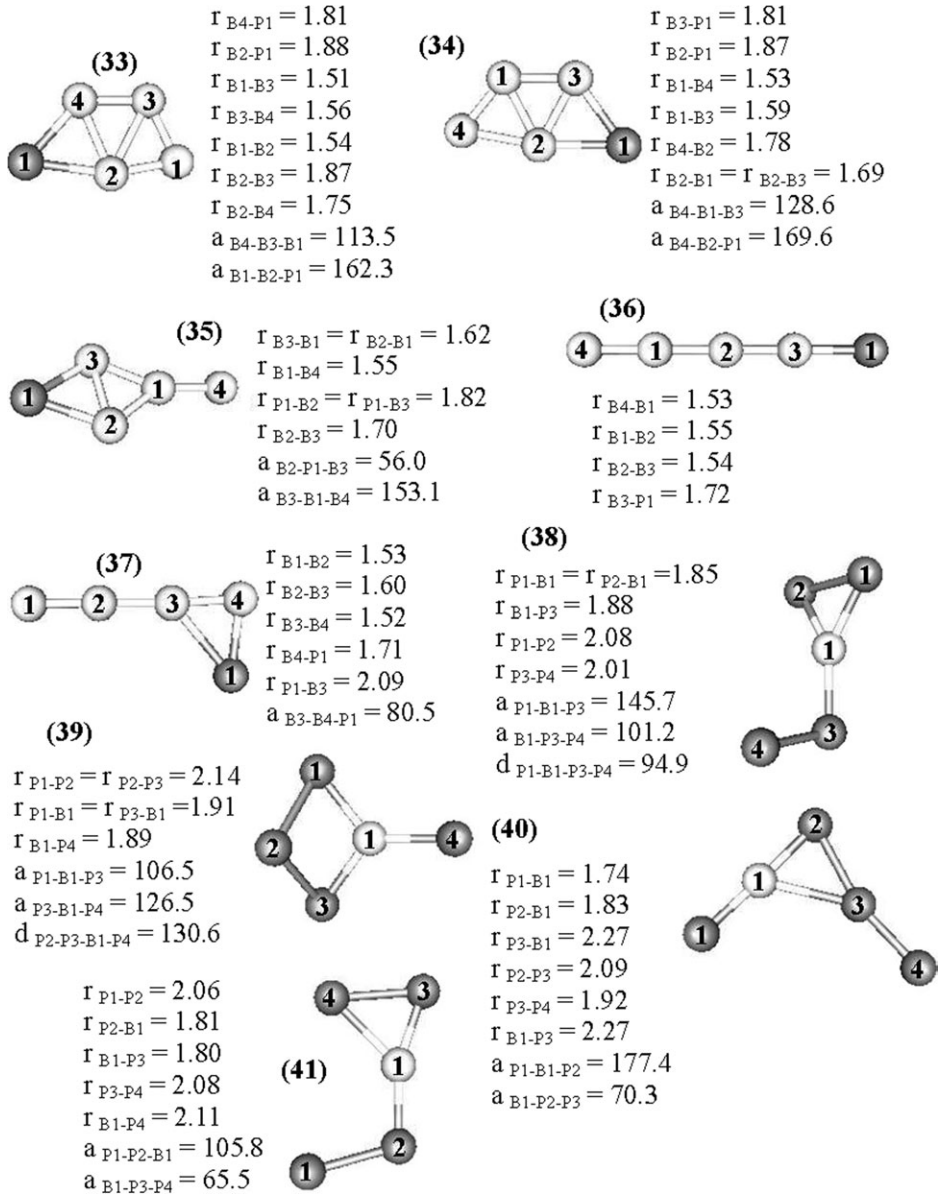

Figure 5. Equilibrium geometries of the stable B_4P and BP_4 pentatomic aggregates. White and gray circles are boron and phosphorus atoms, respectively. Numbers in parenthesis are the cluster labels, see text and Table 3. Equilibrium bond distances, *r*, are indicated in Å and bond angles, *a*, and torsion angles, *d*, are shown in degrees, respectively. Bond angles not shown are equal to 180○. Torsion angles are not provided in the case of planar aggregates.

and a decrease in the number of P—P bonds. The **8** → **16** route, conversely, is formed after an electrophilic attack of a P atom to a B—P bond followed by an increase in the number of B—P bonds and the formation of a P—P bond. Both the change in the number of P—P bonds in the different routes and the criterion of maximum increase in the atomization energy seem to favor the **6** → **16** growing path. Conformer **17** could grow whether from conformer **6** or from conformer **8**. Although the maximum increase in the atomization energy is observed for the **6** → **17** growing route, it can be deduced from the equilibrium structures, see Figures 2 and 3, that two bonds should be broken at least to go from **6** to **17**, suggesting that non-negligible energy barriers could be involved in the growing process. Instead, a simple electrophilic attack of a P atom to a B—P bond originates conformer **17** from **8**. Thus, it is proposed that conformer **17** grows from conformer **8** after an important atomic charge rearrangement takes place. Conformer **24** could grow from **8** or from **14**. It can be seen from Figures 2 and 4 that the **8** → **24** route can be described as an initial electrophilic attack of a B atom to the B—B bond followed by a geometry distortion that leads to the formation of four new bonds with an important rearrangement of MEP-derived atomic charges on the B atoms. Conversely, the growing of **24** from **14** occurs as a consequence of an electrophilic attack of a P atom to a B—B bond followed by a rearrangement of the atomic charges. The criterion of maximum increase in the atomization energy favors the growing of conformer **24** from **8**. Conformer **33** grows from **14** after an electrophilic attack of a B atom to a B—B bond followed by an important MEP-derived atomic charges rearrangement, even involving the P atom, which is the farthest one from the site of the attack. Interestingly, the four pentatomic species considered are characterized by a doublet electronic state. In conformers **16**, **17**, and **24**, the unpaired electron is mainly localized on P atoms, whereas in **33** the unpaired electron is almost equally distributed between the P atom and the B atoms in the aggregate.

Table 4. MEP-derived atomic charges, in units of |e|, and SD per atom as obtained from NBO calculations (see text) in atomic units and in parenthesis, for the stable B/P diatomic and triatomics found in this work.

	B		P	
	1	2	1	2
1	0.04 (1.16)		−0.04 (0.84)	
2	−0.06 (−0.16)		0.03 (0.59)	0.03 (0.59)
3	−0.09 (0.27)		0.06 (0.01)	0.03 (0.73)
4	−0.08 (0.92)	0.04 (0.11)	0.04 (−0.03)	
5	0.20 (1.27)	−0.20 (0.36)	−0.007 (−0.66)	

Numbers in rows are labels to identify conformers, numbers in columns are labels to identify atoms in conformers, see Figure 1.

Table 5. MEP-derived atomic charges, in units of |e|, and SD per atom as obtained from NBO calculations (see text) in atomic units and in parenthesis, for the stable B/P tetratomics found in this work.

	B			P		
	1	2	3	1	2	3
6	0.09			−0.10	0.12	−0.10
7	−0.08			0.07	0.08	−0.06
8	0.002 (−0.11)	0.002 (−0.11)		−0.002 (1.11)	−0.002 (1.11)	
9	−0.02 (−0.11)	−0.006 (0.19)		−0.0003 (1.53)	0.03 (0.11)	
10	0.007 (0.39)	−0.03 (1.53)		0.01 (0.06)	0.01 (0.06)	
11	−0.04 (1.03)	−0.04 (1.03)		0.04 (−0.03)	0.04 (−0.03)	
12	−0.19 (0.55)	−0.19 (0.55)		0.19 (0.45)	0.19 (0.45)	
13	−0.008 (0.84)	−0.004 (0.84)		0.01 (−0.12)	−0.0003 (0.41)	
14	−0.06 (0.87)	0.001 (0.54)	0.002 (0.54)	0.05 (−0.01)		
15	0.08 (1.59)	0.02 (0.84)	−0.07 (−0.22)	−0.04 (−0.22)		

Numbers in rows are labels to identify conformers, numbers in columns are labels to identify atoms in conformers, see Figure 2.

- **1** → **4** → **14** → **33**
- **1** → **4** → **14** → **24**
- **1** → **2** → **8** → **24**

It can be deduced from the paths above and the preceding discussion that the growing mechanism in small B—P aggregates is dominated by electrophilic attacks of B atoms to B—B and B—P bonds. The exceptions are the **14** → **24** path, which is characterized by an electrophilic attack of a P atom to a B—B bond and the **1** → **2** path, which is described as a nucleophilic attack of a P atom to a B atom. Changes in electron spin multiplicities and electron localization during growing are difficult to rationalize.

Table 6. MEP-derived atomic charges, in units of |e|, and SD per atom as obtained from NBO calculations (see text) in atomic units and in parenthesis, for the stable B/P pentatomics found in this work.

#	B				P			
	1	2	3	4	1	2	3	4
16	0.03 (0.10)	0.08 (0.13)			−0.01 (0.41)	−0.03 (0.37)	−0.08 (0.00)	
17	0.22 (−0.01)	−0.16 (0.16)			0.001 (0.04)	−0.06 (0.78)	0.002 (0.04)	
18	−0.03 (0.21)	−0.07 (0.79)			0.05 (−0.05)	−0.001 (0.08)	0.05 (−0.05)	
19	0.04 (0.10)	0.12 (−0.04)			0.01 (0.05)	0.01 (0.05)	−0.19 (0.84)	
20	0.04 (0.65)	0.04 (0.65)			−0.06 (−0.08)	−0.03 (0.13)	0.007 (1.91)	
21	0.24 (0.15)	−0.04 (0.94)			−0.13 (1.76)	−0.03 (0.10)	−0.03 (0.10)	
22	0.11 (0.14)	−0.11 (1.15)			−0.02 (0.43)	−0.01 (0.85)	0.03 (0.44)	
23	−0.11 (0.56)	−0.11 (0.56)			0.12 (−0.01)	0.05 (−0.06)	0.05 (−0.06)	
24	−0.03 (0.06)	0.07 (−0.06)	−0.03 (0.04)		−0.01 (0.50)	−0.004 (0.50)		
25	0.11 (0.06)	0.04 (0.02)	−0.04 (0.93)		−0.0001 (−0.02)	−0.11 (0.01)		
26	0.18 (0.22)	−0.17 (−0.06)	0.08 (0.14)		−0.11 (0.69)	0.01 (−0.02)		
27	−0.17 (0.07)	0.30 (−0.30)	−0.17 (0.06)		0.02 (0.59)	0.02 (0.59)		
28	0.04 (−0.16)	−0.14 (0.56)	0.08 (0.05)		0.01 (0.67)	0.01 (−0.08)		
29	−0.04 (0.94)	−0.04 (0.01)	0.07 (0.05)		0.10 (−0.03)	−0.08 (0.02)		
30	0.004 (1.78)	−0.17 (1.04)	0.22 (0.01)		−0.03 (0.08)	−0.03 (0.08)		
31	−0.09 (0.80)	0.49 (0.15)	−0.32 (0.09)		−0.04 (0.01)	−0.04 (0.01)		
32	−0.09 (0.01)	0.15 (0.22)	−0.10 (0.76)		0.02 (0.01)	0.02 (0.01)		
33	0.04 (0.35)	−0.02 (−0.05)	−0.08 (0.21)	0.09 (−0.10)	−0.03 (0.62)			
34	−0.09 (0.36)	0.19 (0.36)	0.11 (0.45)	−0.10 (1.28)	−0.10 (0.54)			
35	−0.08 (0.41)	−0.01 (0.51)	−0.01 (0.50)	0.11 (1.35)	0.002 (0.19)			
36	−0.08 (0.98)	0.13 (−0.28)	−0.12 (−0.18)	0.10 (1.58)	−0.02 (0.91)			
37	−0.03 (1.72)	0.14 (1.07)	−0.16 (−0.06)	0.04 (0.22)	0.005 (0.05)			
38	0.23 (0.06)				−0.02 (0.00)	−0.13 (0.04)	−0.02 (0.00)	−0.05 (0.93)
39	0.19 (0.06)				−0.05 (0.69)	0.05 (−0.10)	−0.05 (0.69)	−0.14 (1.76)
40	0.04 (0.00)				−0.10 (0.83)	0.08 (0.22)	−0.04 (0.00)	0.02 (0.04)
41	0.004 (1.40)				−0.03 (1.40)	−0.05 (0.09)	0.06 (0.01)	0.01 (1.04)

Numbers in rows are labels to identify conformers, numbers in columns are labels to identify atoms in conformers, see Figures 3–5.

The previous analysis indicates that five patterns could describe the form in which small B—P clusters grow, namely, **1** → **2** → **6** → **16**, **1** → **2** → **8** → **17**, **1** → **2** → **8** → **24**, **1** → **4** → **14** → **24**, and **1** → **4** → **14** → **33**. The first two growing paths show an increase in the atomization energy of about 1.60 eV/at when passing from **1** to **16** and to **17**. Conversely, the last three growing patterns exhibit an increase in the atomization energy of about 1.90 eV/at when passing from **1** to **24** and to **33**. According to these differences, it is proposed as the most probable growing paths for small B—P clusters are

Conclusions

Geometric features of B_nP_m ($n = 1$–4, $m = 1$–4, $n + m \leq 5$) were studied in this work within the framework of the density functional theory. The growing pattern of the most stable aggregates was rationalized with the aid of useful tools obtained from calculations.

Present results indicate that small clusters formed by B and P tend to adopt bidimensional geometries in most cases. The most stable structures found for B_2P, B_3P, and B_4P agree quite well with results reported previously. For B_2P_2, a linear

geometry is found to be more stable than the rhombus-like structure reported previously elsewhere. Several stable geometries for BP_4 are reported for the first time. It is proposed that the higher atomization energies are closely related to the existence both of B—P and of B—B bonds, whereas short P—P bonds are responsible for the relative lower atomization energies.

The growing pattern of small B/P clusters is governed mainly by electrophilic attacks of an incoming B atom to B—P or B—B bonds present in the aggregate of smaller size. The electrophilic attack of an incoming P atom to a B—B bond seems to be an alternative for growing when clusters are saturated with B atoms. It was found that atomic charges derived from MEPs are useful to describe the growing patterns whether in terms of nucleophilic or in terms of electrophilic attacks. Conversely, changes in electron multiplicity are difficult to rationalize.

Acknowledgments

VFC is a fellow of CONICET. RPD is member of the Scientific Research Career of CONICET.

Keywords: B/P clusters · growing pattern · density functional theory

How to cite this article: V. Ferraresi Curotto and R. Pis Diez, *Int. J. Quantum Chem.* **2012,** *112*, 3261–3268. DOI: 10.1002/qua.24194

[1] M. Odawara, T. Udagawa, G. Shimaoka, *Jpn. J. Appl. Phys.* **2005**, *44,* 681.
[2] Y. Kumashiro, *J. Mater. Res.* **1990**, *5,* 2933.
[3] R. Linguerri, N. Komiha, R. Oswald, A. Mitrushchenkov, P. Rosmus, *Chem. Phys.* **2008**, *346,* 1.
[4] Y. Qu, W. Ma, X. Bian, H. Tang, W. Tian, *Int. J. Quantum Chem.* **2006**, *106,* 960.
[5] R. Shi, J. Shao, C. Wang, X. Zhu, X. Lu, *J. Mol. Model.* **2010**, *17,* 1007.
[6] S. Burrill, F. Grein, *J. Mol. Struct. (THEOCHEM)* **2005**, *757,* 137.
[7] Z. Gan, D. J. Grant, R. J. Harrison, D. A. Dixon, *J. Chem. Phys.* **2006**, *125,* 124311.
[8] P. Hohenberg, W. Kohn, *Phys. Rev.* **1964**, *136,* B864.
[9] W. Kohn, L. J. Sham, *Phys. Rev.* **1965**, *140,* A1133.
[10] R. Parr, W. Yang, Density Functional Theory of Atoms and Molecules, Oxford University Press, New York, **1989**.
[11] A. Becke, *J. Chem. Phys.* **1993**, *98,* 5648.
[12] C. Lee, W. Yang, R. G. Parr, *Phys. Rev.* **1988**, *B 37,* 785.
[13] T. H. Dunning, Jr., *J. Chem. Phys.* **1989**, *90,* 1007.
[14] T. H. Dunning, Jr., *J. Mol. Struct. (THEOCHEM)* **1996**, *388,* 339.
[15] V. Ferraresi Curotto, R. Pis Diez, *Comput. Math. Sci.* **2011**, *50,* 3390.
[16] U. C. Singh, P. A. Kollman, *J. Comput. Chem.* **1984**, *5,* 129.
[17] B. H. Besler, K. M. Merz, Jr., P. A. Kollman, *J. Comput. Chem.* **1990**, *11,* 431.
[18] A. E. Reed, L. A. Curtiss, F. Weinhold, *Chem. Rev.* **1988**, *88,* 899.
[19] M. J. Frisch, G. W. Trucks, H. B. Schlegel, G. E. Scuseria, M. A. Robb, J. R. Cheeseman, J. A. Montgomery, Jr., T. Vreven, K. N. Kudin, J. C. Burant, J. M. Millam, S. S. Iyengar, J. Tomasi, V. Barone, B. Mennucci, M. Cossi, G. Scalmani, N. Rega, G. A. Petersson, H. Nakatsuji, M. Hada, M. Ehara, K. Toyota, R. Fukuda, J. Hasegawa, M. Ishida, T. Nakajima, Y. Honda, O. Kitao, H. Nakai, M. Klene, X. Li, J. E. Knox, H. P. Hratchian, J. B. Cross, V. Bakken, C. Adamo, J. Jaramillo, R. Gomperts, R. E. Stratmann, O. Yazyev, A. J. Austin, R. Cammi, C. Pomelli, J. W. Ochterski, P. Y. Ayala, K. Morokuma, G. A. Voth, P. Salvador, J. J. Dannenberg, V. G. Zakrzewski, S. Dapprich, A. D. Daniels, M. C. Strain, O. Farkas, D. K. Malick, A. D. Rabuck, K. Raghavachari, J. B. Foresman, J. V. Ortiz, Q. Cui, A. G. Baboul, S. Clifford, J. Cioslowski, B. B. Stefanov, G. Liu, A. Liashenko, P. Piskorz, I. Komaromi, R. L. Martin, D. J. Fox, T. Keith, M. A. Al-Laham, C. Y. Peng, A. Nanayakkara, M. Challacombe, P. M. W. Gill, B. Johnson, W. Chen, M. W. Wong, C. Gonzalez, J. A. Pople, Gaussian 03, revision d.01 [computer software], Gaussian, Inc., Pittsburgh PA, **2004**.
[20] L. Laaksonen, *J. Mol. Graph.* **1992**, *10,* 33.
[21] D. L. Bergman, L. Laaksonen, A. Laaksonen, *J. Mol. Graph. Model.* **1997**, *15,* 301.

Received: 16 November 2011
Revised: 2 May 2012
Accepted: 3 May 2012
Published online on 5 June 2012